How to cite:
doi.org/10.1002/anie.202303929

2D Materials

High-throughput Synthesis of Solution-Processable van der Waals Heterostructures through Electrochemistry

Huanhuan Shi[+], Mengmeng Li[+], Shuai Fu[+], Christof Neumann, Xiaodong Li, Wenhui Niu, Yunji Lee, Mischa Bonn, Hai I. Wang, Andrey Turchanin, Ali Shaygan Nia, Sheng Yang,* and Xinliang Feng**

Abstract: Two-dimensional van der Waals heterostructures (2D vdWHs) have recently gained widespread attention because of their abundant and exotic properties, which open up many new possibilities for next-generation nanoelectronics. However, practical applications remain challenging due to the lack of high-throughput techniques for fabricating high-quality vdWHs. Here, we demonstrate a general electrochemical strategy to prepare solution-processable high-quality vdWHs, in which electrostatic forces drive the stacking of electrochemically exfoliated individual assemblies with intact structures and clean interfaces into vdWHs with strong interlayer interactions. Thanks to the excellent combination of strong light absorption, interfacial charge transfer, and decent charge transport properties in individual layers, thin-film photodetectors based on graphene/In_2Se_3 vdWHs exhibit great promise for near-infrared (NIR) photodetection, owing to a high responsivity (267 mA W^{-1}), fast rise (72 ms) and decay (426 ms) times under NIR illumination. This approach enables various hybrid systems, including graphene/In_2Se_3, graphene/MoS_2 and graphene/$MoSe_2$ vdWHs, providing a broad avenue for exploring emerging electronic, photonic, and exotic quantum phenomena.

Introduction

Two-dimensional (2D) materials are emerging building blocks for next-generation quantum nanomaterials.[1] Van der Waals integration of 2D materials into artificial heterostructures allows for combining diverse properties and exploring exotic phenomena that are not previously possible.[2] For example, the Hofstadter butterfly effect and topological currents have been observed in the vdWHs of graphene and hexagonal boron nitride (hBN) owing to their spectrum reconstruction.[3] The study of tunneling and drag effects is possible in the closely combined 2D crystals.[4] Moreover, the optically active heterostructures have been prepared *via* stacking semiconducting monolayers.[5] The extended range of functionalities of vdWHs yields many emergent applications. For instance, the graphene transistors with the highest mobility have been achieved by encapsulating graphene with hBN.[6] Photovoltaic and light-emitting devices have been demonstrated by combining optically active semiconducting layers with graphene as transparent electrodes.[7]

Thus far, mechanical exfoliation and stacking is the most widely-used method for producing the highest-quality vdWHs.[1c,2c,8] While this is critical for fundamental studies, it is inherently difficult to scale up for practical device applications. Liquid phase exfoliation and assembly is an effective method for bulk production of vdWHs.[8,9] How-

[*] Dr. H. Shi,[+] Dr. X. Li, Dr. W. Niu, Dr. A. Shaygan Nia, Prof. X. Feng
Center for Advancing Electronics Dresden (cfaed) and Department of Chemistry and Food Chemistry, Technische Universität Dresden
Mommsenstrasse 4, 01062 Dresden (Germany)
E-mail: ali.shaygan_nia@tu-dresden.de
xinliang.feng@tu-dresden.de

Dr. X. Li, Dr. W. Niu, Dr. A. Shaygan Nia, Prof. X. Feng
Max Planck Institute for microstructure physics
Weinberg 2, 06120 Halle (Germany)

Dr. S. Yang
Frontiers Science Center for Transformative Molecules, School of Chemistry and Chemical Engineering, Shanghai Jiao Tong University
200240 Shanghai (China)
E-mail: sheng.yang@sjtu.edu.cn

Prof. M. Li[+]
Key Laboratory of Microelectronic Devices and Integrated Technology, Institute of Microelectronics, Chinese Academy of Sciences
100029 Beijing (China)
and
University of Chinese Academy of Sciences
100049 Beijing (China)

S. Fu,[+] Y. Lee, Prof. M. Bonn, Dr. H. I. Wang
Max Planck Institute for Polymer Research
Ackermannweg 10, 55128 Mainz (Germany)

Dr. C. Neumann, Prof. A. Turchanin
Institute of Physical Chemistry and Center for Energy and Environmental Chemistry Jena (CEEC Jena), Friedrich Schiller University Jena
Lessingstrasse 10, 07743 Jena (Germany)

[+] These authors contributed equally to this work.

ever, the harsh sonication process causes a large number of defects and contaminates the surface; the constituted layers are usually randomly mixed, resulting in vdWHs with low quality and inferior physicochemical properties.[10] Direct growth methods, including chemical vapor deposition and epitaxial growth, are also popular for the scalable preparation of high-quality vdWHs.[11] Nonetheless, the diversity of vdWHs is limited by the lattice mismatch between the two subsequent grown crystalline layers.[12] Although considerable efforts have been made to construct diverse vdWHs, it remains a great challenge to fabricate vdWHs in a manner that combines several advantages of high quality, high efficiency, and solution processability.

Here, we demonstrate a general strategy for the large-scale preparation of high-quality vdWHs based on the rational design of in-solution electrolytic chemistry. Careful choice of charge carriers and solvents enables simultaneous exfoliation of two different vdW crystals into their corresponding defect-free bilayers or monolayers. Afterwards, these oppositely charged 2D sheets self-assemble into vdWHs driven by electrostatic interactions. Thanks to the developed electrolyte formulation, the produced vdWHs exhibit intact structures, clean interfaces, and strong interlayer coupling, which contribute to efficient interfacial charge transfer and outstanding photodetection performance in the NIR region. Furthermore, the universality of this method has been demonstrated by the successful preparation of graphene/In_2Se_3, graphene/MoS_2 and graphene/$MoSe_2$ vdWHs, opening up new avenues for the development of emerging nanoelectronics, including printable electronics.

Results and Discussion

Figure 1 and Figure S1 conceptually compare different strategies for fabricating vdWHs, including the conventional mechanical-based exfoliation/stacking and liquid-phase mixing methods and the newly proposed electrochemical dual-ion exfoliation approach. Compared with mechanical-based stacking and liquid-phase mixing methods, our process has the advantages of high quality and large quantity. At the heart of this approach, the design of the electrolyte (e.g., charge carriers and solvents) plays a crucial role in the electrochemical exfoliation process and determines the structural integrity and interfacial cleanliness of the constituted 2D layers. After careful comparison and screening of many possible ionic compounds, we use tetra-*n*-butylammonium bisulfate (TBA HSO_4) as the electrolyte salt in our work because the size of TBA^+ (0.86 nm) matches well with the interlayer spacing of most vdW crystals (0.6–1 nm) and SO_4^{2-} is the most popular intercalant for anodic

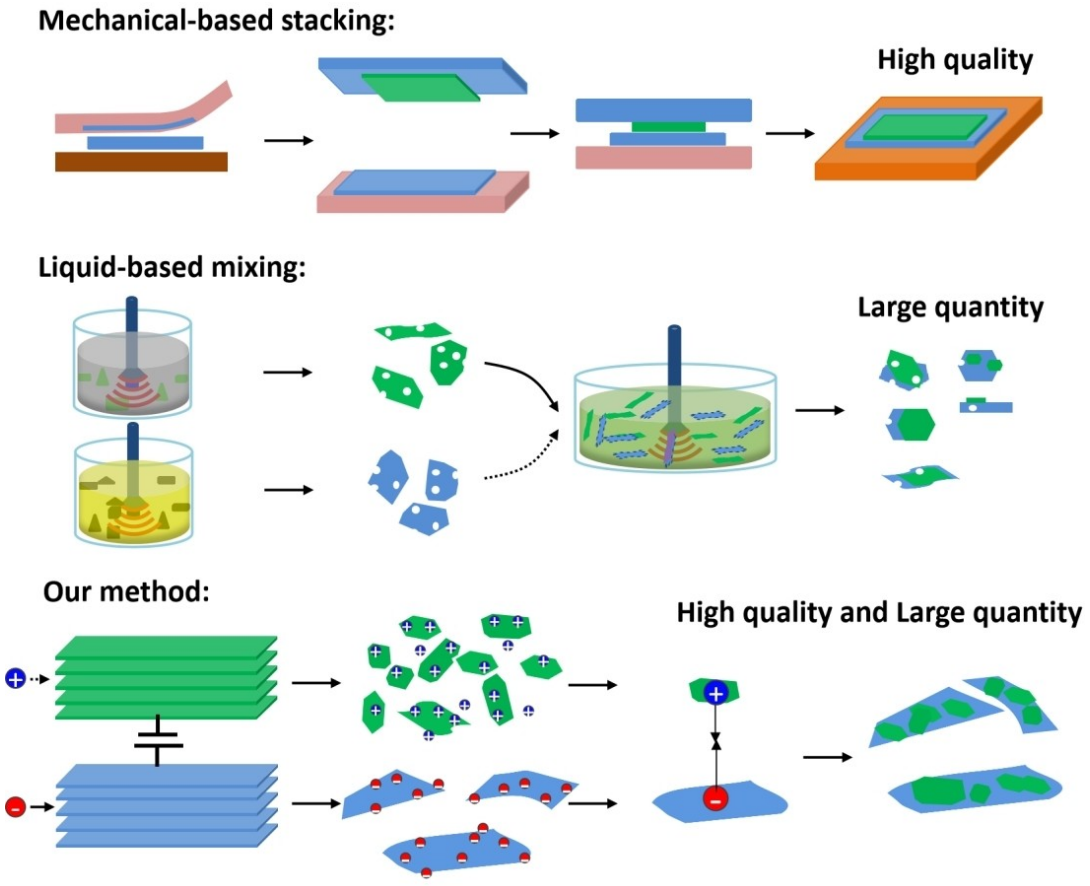

Figure 1. Schematic illustration of different strategies for fabricating vdWHs.

exfoliation.[13] Moreover, TBA HSO_4 shows good solubility in common organic solvents or water to offer high concentration. Another key parameter that affects electrolyte performance is the solvent. Here we employ a mixture of acetonitrile and water as the dispersion solvent for the following reasons: (i) the high dielectric constant of water (80.1) helps stabilize charges in solutions; (ii) the low viscosity of acetonitrile (0.34×10^{-3} Pa s) facilitates ion migration; (iii) residual contaminants on 2D surfaces can be easily removed due to their low boiling points (i.e., 81 °C for acetonitrile and 100 °C for water); and (iv) the dielectric constant and viscosity of the mixture can be fine-tuned by controlling their mixing ratio, providing another degree of freedom for regulating the self-assembly of the exfoliated 2D layers and optimizing their quality.

Graphene/In_2Se_3 vdWHs were selected as a prototype system to demonstrate the electrochemical dual-ion exfoliation approach due to their fascinating electronic band structures (e.g., the direct band gap of semiconducting monolayer In_2Se_3 and the Dirac cone of graphene) and exceptional optoelectronic applications.[14] Toward this end, bulk vdW crystals of graphite and In_2Se_3 were placed at the anode and cathode, respectively (Figure S2). To achieve efficient dual-ion exfoliation, we first compared the delamination performance of TBA HSO_4 in acetonitrile/water mixed solvents with different mixing ratios (e.g., 1:1, 3:1, 9:1, 19:1, 19.5:0.5). As shown in Figure S3, obvious expansion of In_2Se_3 crystals was observed when the ratio of acetonitrile and water was increased to 19:1, while other low ratios did not cause any visible exfoliation. Furthermore, the ratios of 19:1 and 19.5:0.5 were tested for anodic delamination of graphite. We found that graphite showed efficient exfoliation at a ratio of 19:1, while the expansion under the ratio of 19.5:0.5 was limited (Figure S4). Therefore, we selected a volume ratio of 19:1 as the optimal value.

We further characterized the morphology of the individually exfoliated In_2Se_3 and graphene made from the above-designed hybrid electrolyte (Figure 2a, d and Figure S5). According to the atomic force microscopy (AFM) image, the average thickness of In_2Se_3 nanosheets is ≈1.5 nm (82 %), corresponding to the monolayer thickness (Figure S6). They are much thinner than the In_2Se_3 sheets (3–10 nm) obtained by wet-chemical methods,[15] probably due to the edge oxidation of In_2Se_3 crystal with the help of water during the exfoliation process. Specifically, the intercalation of TBA^+ ions into In_2Se_3 crystals becomes more favorable when the interlayer spacing at the edges increases. Besides, the composition and structure of the exfoliated In_2Se_3 flakes were investigated by X-ray photoelectron spectroscopy (XPS, Figure S7) and high-resolution transmission electron microscope (HR-TEM, Figure 2b), respectively. The peak fits of In 3d and Se 3d were consistent with those of the original In_2Se_3. A small content of In_xO_y was observed, most likely caused by partial oxidation at the edges. HR-TEM image collected from the inner surface of In_2Se_3 sheets revealed clear and well-defined lattice fringes, confirming the exfoliation of high-quality In_2Se_3 sheets. On the other hand, bilayer graphene sheets were exfoliated in the same electrolyte (Figure 2d). The exfoliated graphene sheets exhibited much lower oxygen content than those produced from aqueous electrolytes, which can be attributed to the

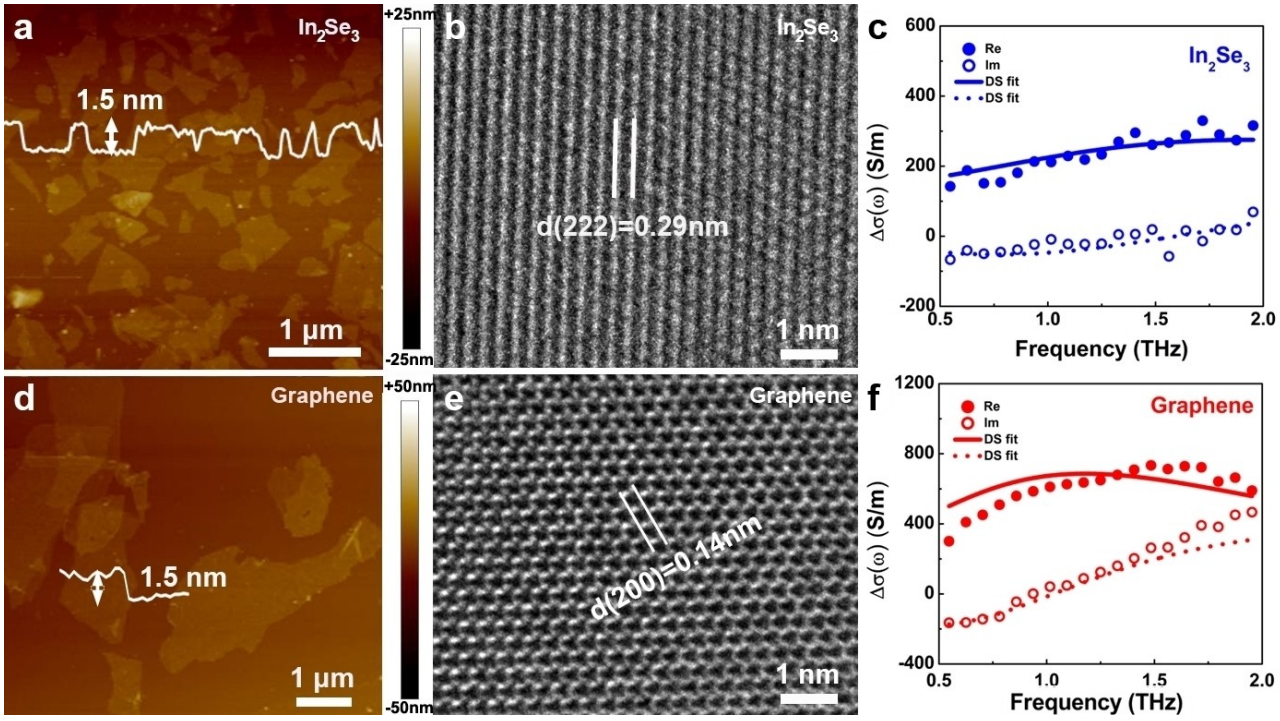

Figure 2. Characterizations of electrochemically exfoliated In_2Se_3 and graphene sheets. a), d) AFM images, b), e) High-resolution TEM images, and c), f) Frequency-resolved complex THz photoconductivity spectra.

reduced amount of oxide radicals (e.g., HO•) generated from water electrolysis (Figure S8).[13] The obtained graphene sheets showed a typical hexagonal honeycomb lattice in the HR-TEM image (Figure 2e).

The charge transport properties of the exfoliated In_2Se_3 and graphene sheets were investigated by time-resolved THz spectroscopy (TRTS). Following above-band gap excitations (800 nm for exfoliated graphene and 400 nm for exfoliated In_2Se_3), the exfoliated graphene showed a transient increase in conductivity followed by rapid recombination within a few ps (Figure S9), whereas the exfoliated In_2Se_3 exhibited a much longer carrier lifetime, on the order of tens of ps. The frequency-resolved photoconductivity ($\Delta\sigma(\omega)$) of exfoliated graphene and In_2Se_3 are shown in Figures 2c and f. The obtained $\Delta\sigma(\omega)$ can be well described by the Drude–Smith (DS) mode, which has been widely used to interpret charge transport in various nanomaterial systems subject to the backscattering effect (See details in Supporting Information).[16] The *dc* mobilities of graphene and In_2Se_3 can be roughly estimated as $1400 \pm 100\ cm^2V^{-1}s^{-1}$ and $130 \pm 20\ cm^2V^{-1}s^{-1}$, respectively. We note that the estimated charge mobility of graphene is higher than that of graphene nanosheets produced by electrochemical anodic exfoliation in water,[17] validating the high-quality graphene obtained here.

The successful exfoliation of individual graphene and In_2Se_3 sheets with excellent structural integrity and charge transport properties prompted us to further explore the

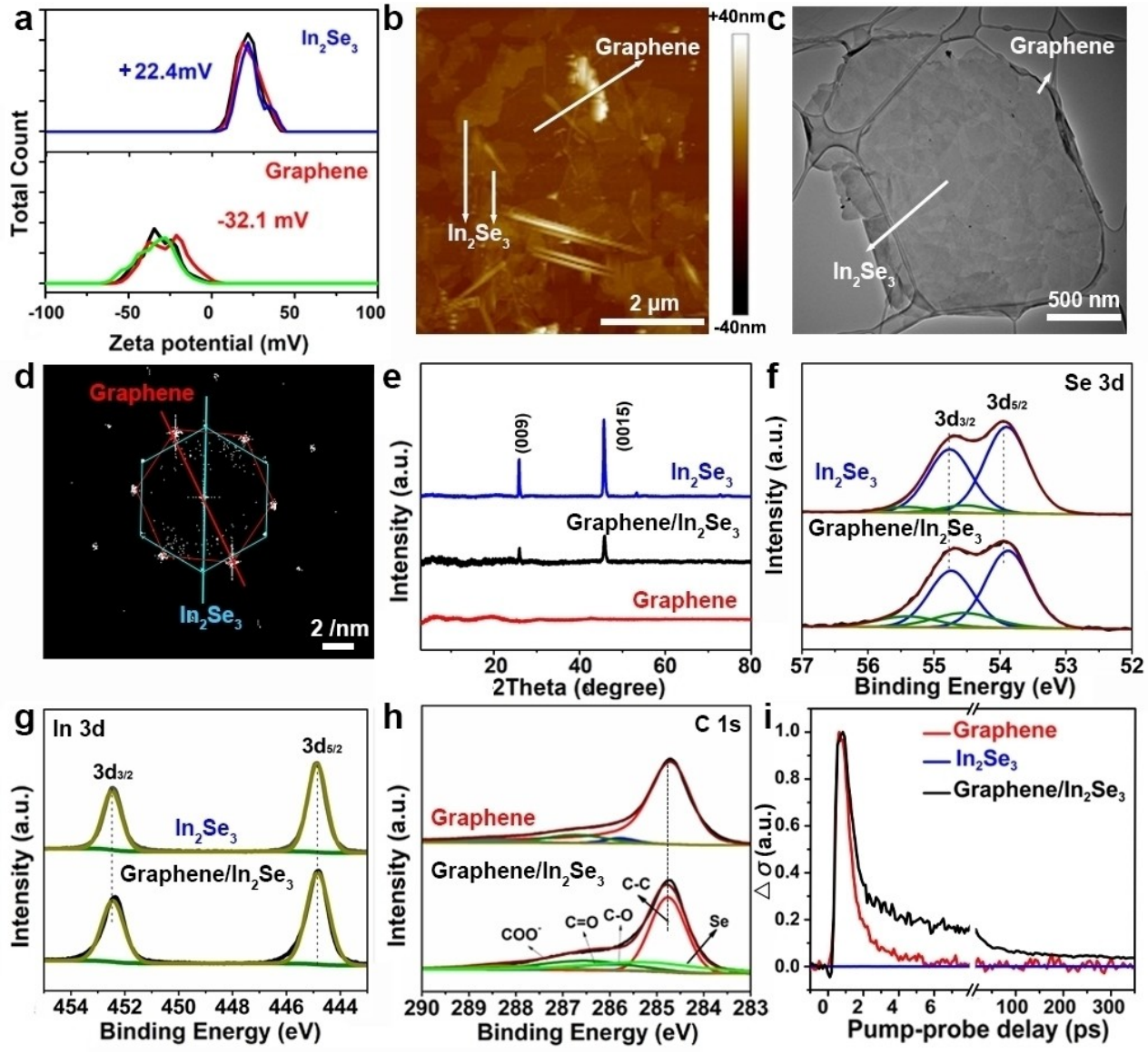

Figure 3. Characterizations of the formed graphene/In_2Se_3 vdWHs. a) Zeta potentials of exfoliated In_2Se_3 and graphene, respectively. b) AFM image, c) TEM image, d) SAED patterns of graphene/In_2Se_3 vdWHs. e) XRD patterns and f)–h) High-resolution XPS of Se 3d, In 3d, and C 1s of In_2Se_3, graphene/In_2Se_3 vdWHs, and graphene. i) Normalized time-resolved THz photoconductivity of graphene, In_2Se_3, and graphene/In_2Se_3 vdWHs under 800 nm excitation.

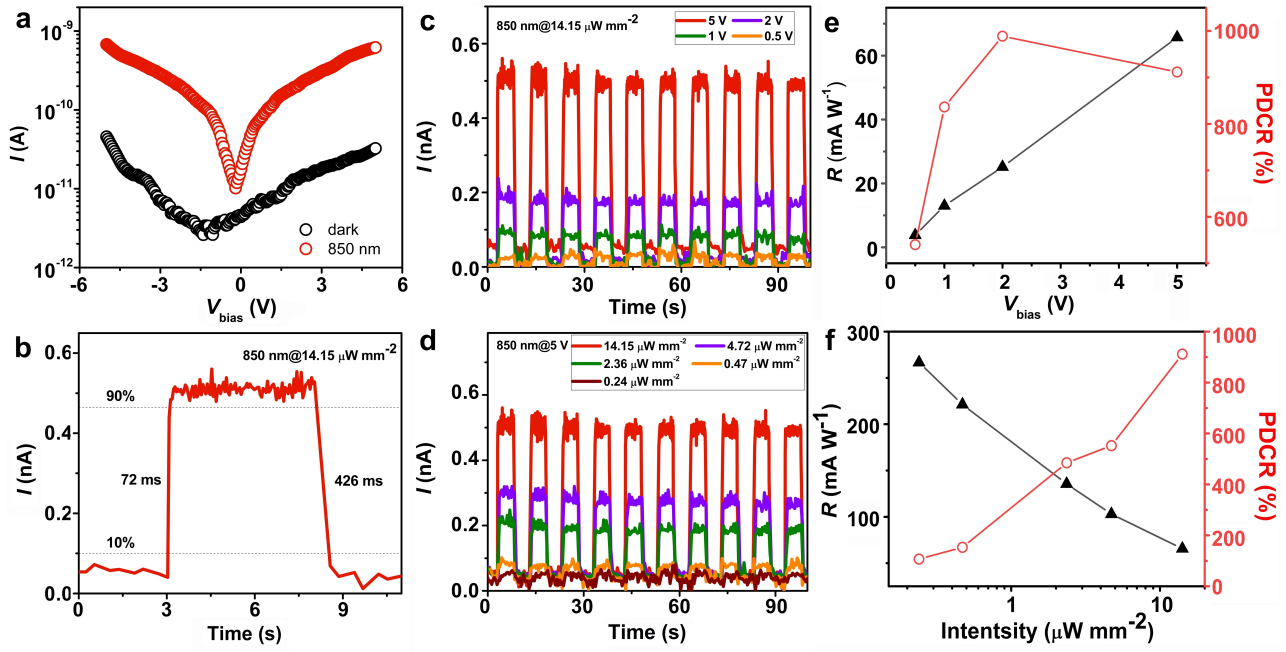

Figure 4. NIR photodetectors based on graphene/In_2Se_3 vdWHs. a) *I–V* curves of graphene/In_2Se_3 photodetector with (ON) and without (OFF) 850 nm illumination. b) Response time of the thin-film device. c) Photoresponse of graphene/In_2Se_3 devices at different voltages under 850 nm illumination. d) Photoresponse of graphene/In_2Se_3 devices at different illumination densities (850 nm). e, f) Responsivity (R) and photo-to-dark current ratio (PDCR) curves of graphene/In_2Se_3 photodetector as a function of bias voltage and illumination density (850 nm).

feasibility of dual-ion exfoliation and one-pot assembly of high-quality vdWHs. Specifically, negatively charged sulfate (SO_4^{2-}) and positively charged tetra-*n*-butylammonium (TBA^+) are expected to adsorb on the graphene and In_2Se_3 surfaces, respectively, during the dual-ion exfoliation process. This can, in principle, initiate a spontaneous assembly process driven by electrostatic interactions (Figure S10). To test this hypothesis, the exfoliated In_2Se_3 and graphene sheets were collected separately, and their surface polarity was examined by Zeta potential measurements.

As shown in Figure 3a, the surface of In_2Se_3 is positively charged (+22.4 mV), while that of graphene is negatively charged (−32.1 mV). The oppositely charged surfaces provide the basis for the subsequent self-assembly into high-concentration vdWHs (2 mg mL^{-1}) in solution. The structure and morphology of the products were examined by scanning electron microscopy (SEM, Figure S11), AFM (Figure 3b), and TEM (Figure 3c,d). These images revealed a typical vertically stacked graphene/In_2Se_3 vdWH made of many monolayer In_2Se_3 flakes assembled on the surface of bilayer graphene. Besides, HR-TEM image showed a clean interface with graphene on top in the formed vdWH (Figure S12). The corresponding selected area electron diffraction (SAED) pattern (Figure 3d) exhibited two different hexagonal patterns, which can be attributed to graphene (yellow) and In_2Se_3 (red), respectively. Element mapping confirmed the presence of In, Se, and C atoms in the graphene/In_2Se_3 vdWHs (Figure S13).

To evaluate the crystal structures and interfacial interactions of the formed graphene/In_2Se_3 vdWHs, X-ray diffraction (XRD), XPS, photoluminescence (PL), and Raman spectra were performed. According to the XRD patterns in Figure 3e, the characteristic diffraction peaks of both graphene and In_2Se_3 were well preserved in the vdWHs. The surface chemical compositions of In_2Se_3, graphene/In_2Se_3 vdWHs, and graphene were elucidated by XPS (Figure S14). As depicted in Figure 3f–h, the high-resolution XPS of In 3d included peaks at 444.8 and 452.5 eV, corresponding to the $3d_{5/2}$ and $3d_{3/2}$ components of In^{3+} in pristine In_2Se_3. The peaks of In 3d in graphene/In_2Se_3 vdWHs shifted to lower binding energies by 0.1 eV compared to those of pristine In_2Se_3. Similarly, the Se 3d spectra of graphene/In_2Se_3 vdWHs consisted of peaks at 53.7 and 54.7 eV, associated with Se $3d_{5/2}$ and $3d_{3/2}$, which are 0.1 eV lower than the corresponding peaks in In_2Se_3. In contrast, the C 1s spectra of graphene/In_2Se_3 vdWHs was shifted towards higher binding energies by 0.2 eV compared with those of graphene, indicating a strong interlayer interaction between In_2Se_3 and graphene in the formed vdWHs.[18] This result was also confirmed by PL and Raman measurements.[19] As shown in Figure S15, the exfoliated In_2Se_3 itself exhibits a strong PL peak at around 880 nm upon excitation, while the PL intensity in graphene/In_2Se_3 vdWHs is largely quenched by about 60 %. In Raman spectra, 2D peak of graphene/In_2Se_3 shifts to a high wavenumber compared with that of graphene. According to previous reports,[20] the interaction of graphene and In_2Se_3 would form a type I vdWH (Figure S16), where the Dirac point of graphene is located between the conduction and valence bands of In_2Se_3. Considered that strong interlayer interaction usually causes changes in interfacial charge carrier (e.g., charge separation and recombination) at the

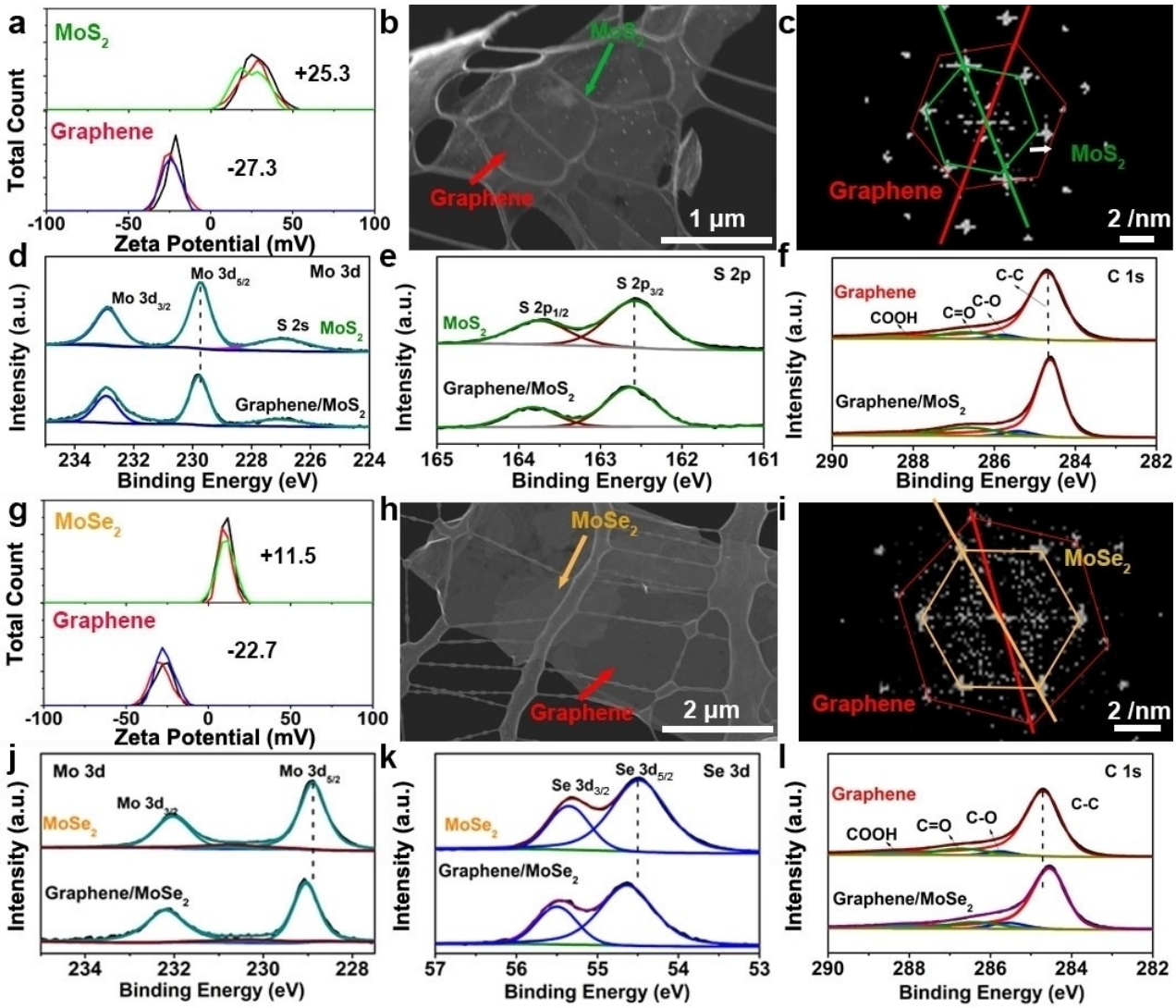

Figure 5. Universality of the proposed electrochemical dual-ion intercalation method. a) Zeta potentials of exfoliated graphene and MoS_2. b), c) TEM images and SAED patterns of graphene/MoS_2 vdWHs. d)–f) High-resolution XPS of Mo 3d, S 2p and C 1s of MoS_2, graphene/MoS_2, and graphene. g) Zeta potentials of exfoliated graphene and $MoSe_2$. h)–i) TEM images and SAED patterns of graphene/$MoSe_2$ vdWHs. j)–l) High-resolution XPS of Mo 3d, Se 3d and C 1s of $MoSe_2$, graphene/$MoSe_2$ vdWHs, and graphene.

graphene/In_2Se_3 vdW interface, we compared the normalized time-resolved photoconductivity of graphene, In_2Se_3, and their vdWHs under the same excitation conditions (800 nm, 1.33 mJ cm^{-2}). As shown in Figure 3i, the photoconductivity of graphene decays to zero on a $\approx$1 ps timescale, while In_2Se_3 shows no photoconductivity within experimental error because the excitation photon energy is below its band gap. For the graphene/In_2Se_3 vdWHs, the photoconductivity dynamics follow a bi-exponential relaxation characterized by fast and slow relaxation components with time constants of $t_1 \approx 2$ ps and $t_2 \approx 50$ ps, respectively. Here, we tentatively attributed the fast photoconductivity decay to the rapid recombination of charge carriers in graphene and the slow photoconductivity decay to the interlayer recombination across graphene/In_2Se_3 interfaces following interfacial charge transfer (CT). In this scenario, photoexcitation generates electrons in the conduction band and holes in the valence band in graphene. These photogenerated charge carriers can have two relaxation pathways: (i) the charge carriers retained in graphene can relax *via* intra-layer recombination (e.g., trapping to defects), and (ii) the charge carriers transferred from graphene to In_2Se_3 can relax *via* interlayer recombination. The occurrence of interfacial CT demonstrates substantial interfacial electronic coupling in graphene/In_2Se_3 vdWHs formed by electrostatic force-induced self-assembly, a prerequisite for exploring their synergistic effects in device applications. Furthermore, the prolonged charge carrier lifetime enabled by interfacial charge separation and the high mobility of graphene allows charge carriers to recirculate many times within a given time, promising for photon-sensing applications.

For that, the prepared graphene/In_2Se_3 vdWHs were integrated into thin-film photodetectors (where the film was 1 μm thick, Figure S17). Figure 4a shows the *I–V* curves of

graphene/In_2Se_3 vdWHs with and without NIR illumination. It was evident that, compared to dark current, the current was enhanced by more than one order of magnitude under 850 nm light illumination. The measured rise and fall times were 72 and 426 ms, respectively (Figure 4b).[15a] Furthermore, we noticed that the performance of the fabricated photodetector was highly dependent on the bias voltage (Figure 4c). The required operation voltage (bias voltage) was significantly reduced compared to the In_2Se_3 photodetector. In particular, an obvious photoresponse to 850 nm light was observed at a bias voltage as low as 0.5 V, substantially decreasing the device's power consumption. The resultant responsivity (R) and photo-to-dark current ratio (PDCR) are summarized in Figure 4e. It was clear that R is almost proportional to the bias voltage, and $R = 66\ mA\,W^{-1}$ was obtained at 5 V, much higher than that of the bare In_2Se_3 photodetector. Besides, the maximum PDCR reaches 990 %. On the other hand, the dependence of photoresponse on light intensity was also investigated (Figures 4d and f).

It was obvious that lower light intensity leads to smaller photocurrents, but a distinguishable photoresponse was achieved even at 850 nm illumination as low as $0.24\ \mu W\,mm^{-2}$. Note that in this case, *R* was noticeably enhanced to $267\ mA\,W^{-1}$, outclassing the performance of previously reported thin-film photodetectors based on transition metal dichalcogenides (Table S1). With increasing light intensity, the enhanced photocurrent and almost constant dark current gave rise to a linear relationship between PDCR and light intensity. Additionally, it was found that the fabricated photodetector based on graphene/In_2Se_3 vdWHs can also detect NIR light at 1050 nm, as shown in Figure S18.

The universality of this strategy was verified by fabricating various graphene-based vdWHs by simply replacing the cathode materials with other vdW crystals, such as MoS_2 and $MoSe_2$, in the developed electrolyte. Likewise, the surfaces of MoS_2 and $MoSe_2$ are positively charged, while graphene is negatively charged (Figure 5a and g). In this way, stable dispersions ($2\ mg\,mL^{-1}$) of graphene/MoS_2 and graphene/$MoSe_2$ vdWHs can be prepared through electrochemical exfoliation and stacking (Figure S19). TEM images, SAED patterns, and EDS mapping (Figure 5b, c, h and i, Figure S20, S21) clearly reveal their well-preserved 2D structure, where several MoS_2 ($MoSe_2$) sheets are assembled with a graphene sheet. The peaks shift in the XPS (Figure 5d–f, Figure 5j–l) confirms the good interlayer interactions in the formed graphene/MoS_2 and graphene/$MoSe_2$ vdWHs.

Conclusion

In summary, we report a general electrochemical dual-ion exfoliation approach for the high-throughput production of solution-processable vdWHs. Various high-concentration vdWH dispersions ($2\ mg\,mL^{-1}$), including graphene/In_2Se_3, graphene/MoS_2, and graphene/$MoSe_2$, were prepared using graphite and different vdW crystals as anode and cathode, respectively. Driven by electrostatic forces, the exfoliated components assemble into artificial vdWHs with extraordinary structural integrity and strongly coupled interfaces, enabling photodetectors with high responsivity and fast response time in the NIR region. Our strategy provides an alternative and facile route to fabricate large-area and high-quality artificial vdWHs, facilitating the exploration of exotic quantum phenomena and the future development of vdWHs-based advanced (opto-) electronics.

Acknowledgements

This work was financially supported by ERC Consolidator Grant on T2DCP, M-ERA-NET project HYSUCAP, SPES3 project funded by German Ministry for Education and Research (BMBF) under Forschung für neue Mikroelektronik (ForMikro) program and GrapheneCore3 881603, National Natural Science Foundation of China (Nos. 22205141, 62074163), Shanghai Pujiang Program (No. 22PJ1408300), the Fundamental Research Funds for the Central Universities of China (22X010201631). The authors thank Dr. Yannan Liu, Dr. Markus Löffler and Dr. Priyanka Sharan for helpful discussions and characterization, and also acknowledge the Center for Advancing Electronics Dresden (cfaed), the Dresden Center for Nanoanalysis (DCN). H.S. and S.F. thank China Scholarship Council (CSC) for financial support. C.N and A.T. acknowledge support by the European Fonds for Regional Development (Europäischer Fonds für Regionale Entwicklung; EFRE-OP 2014–2020; Project No. 2021 FGI 0035, NanoLabXPS) as part of the REACT-EU program as well as DFG SPP2244 "2D Materials—Physics of van der Waals [hetero]structures", Project TU149/13-1. Open Access funding enabled and organized by Projekt DEAL.

Conflict of Interest

The authors declare no conflict of interest.

Data Availability Statement

The data that support the findings of this study are available from the corresponding author upon reasonable request.

Keywords: 2D Semiconductors · Electrochemical Synthesis · NIR Photodetectors · Solution Processability · Van Der Waals Heterostructures

[1] a) K. Novoselov, A. Mishchenko, A. Carvalho, A. Castro Neto, *Science* **2016**, *353*, aac9439; b) Y. Saito, T. Nojima, Y. Iwasa, *Nat. Rev. Mater.* **2016**, *2*, 16094; c) A. K. Geim, I. V. Grigorieva, *Nature* **2013**, *499*, 419; d) N. A. Kumar, M. A. Dar, R. Gul, J.-B. Baek, *Mater. Today* **2015**, *18*, 286.

[2] a) Y. Liu, N. O. Weiss, X. Duan, H.-C. Cheng, Y. Huang, X. Duan, *Nat. Rev. Mater.* **2016**, *1*, 16042; b) K. Kang, K.-H. Lee, Y. Han, H. Gao, S. Xie, D. A. Muller, J. Park, *Nature* **2017**,

550, 229; c) W. J. Yu, Y. Liu, H. Zhou, A. Yin, Z. Li, Y. Huang, X. Duan, *Nat. Nanotechnol.* **2013**, *8*, 952; d) F. Withers, D. Pozo-Zamudio, A. Mishchenko, A. Rooney, A. Gholinia, K. Watanabe, T. Taniguchi, S. J. Haigh, A. Geim, A. Tartakovskii, *Nat. Mater.* **2015**, *14*, 301; e) J. Wang, H. Zhou, S. Li, L. Wang, *Angew. Chem. Int. Ed.* **2023**, *62*, e202218321.

[3] a) B. Hunt, J. D. Sanchez-Yamagishi, A. F. Young, M. Yankowitz, B. J. LeRoy, K. Watanabe, T. Taniguchi, P. Moon, M. Koshino, P. Jarillo-Herrero, *Science* **2013**, *340*, 1427; b) M. Yankowitz, Q. Ma, P. Jarillo-Herrero, B. J. LeRoy, *Nat. Rev. Phys.* **2019**, *1*, 112; c) C. R. Dean, L. Wang, P. Maher, C. Forsythe, F. Ghahari, Y. Gao, J. Katoch, M. Ishigami, P. Moon, M. Koshino, *Nature* **2013**, *497*, 598.

[4] a) D. Ghazaryan, M. T. Greenaway, Z. Wang, V. H. Guarochico-Moreira, I. J. Vera-Marun, J. Yin, Y. Liao, S. V. Morozov, O. Kristanovski, A. I. Lichtenstein, *Nat. Electron.* **2018**, *1*, 344; b) G. Kim, S.-S. Kim, J. Jeon, S. I. Yoon, S. Hong, Y. J. Cho, A. Misra, S. Ozdemir, J. Yin, D. Ghazaryan, *Nat. Commun.* **2019**, *10*, 230; c) A. Mishchenko, J. Tu, Y. Cao, R. V. Gorbachev, J. Wallbank, M. Greenaway, V. Morozov, S. Morozov, M. Zhu, S. Wong, *Nat. Nanotechnol.* **2014**, *9*, 808.

[5] a) P. Rivera, J. R. Schaibley, A. M. Jones, J. S. Ross, S. Wu, G. Aivazian, P. Klement, K. Seyler, G. Clark, N. J. Ghimire, *Nat. Commun.* **2015**, *6*, 6242; b) Y. Deng, Z. Luo, N. J. Conrad, H. Liu, Y. Gong, S. Najmaei, P. M. Ajayan, J. Lou, X. Xu, P. D. Ye, *ACS Nano* **2014**, *8*, 8292.

[6] P. Vabbina, N. Choudhary, A.-A. Chowdhury, R. Sinha, M. Karabiyik, S. Das, W. Choi, N. Pala, *ACS Appl. Mater. Interfaces* **2015**, *7*, 15206.

[7] a) K. Roy, M. Padmanabhan, S. Goswami, T. P. Sai, G. Ramalingam, S. Raghavan, A. Ghosh, *Nat. Nanotechnol.* **2013**, *8*, 826; b) H. Fang, C. Battaglia, C. Carraro, S. Nemsak, B. Ozdol, J. S. Kang, H. A. Bechtel, S. B. Desai, F. Kronast, A. A. Unal, *Proc. Natl. Acad. Sci. USA* **2014**, *111*, 6198; c) R. Cheng, D. Li, H. Zhou, C. Wang, A. Yin, S. Jiang, Y. Liu, Y. Chen, Y. Huang, X. Duan, *Nano Lett.* **2014**, *14*, 5590; d) S. Bellani, A. Bartolotta, A. Agresti, G. Calogero, G. Grancini, A. Di Carlo, E. Kymakis, F. Bonaccorso, *Chem. Soc. Rev.* **2021**, *50*, 11870.

[8] S. J. Haigh, A. Gholinia, R. Jalil, S. Romani, L. Britnell, D. C. Elias, K. S. Novoselov, L. A. Ponomarenko, A. K. Geim, R. Gorbachev, *Nat. Mater.* **2012**, *11*, 764.

[9] a) P. Xiong, F. Zhang, X. Zhang, S. Wang, H. Liu, B. Sun, J. Zhang, Y. Sun, R. Ma, Y. Bando, *Nat. Commun.* **2020**, *11*, 3297; b) X. Zhang, Z. Lai, C. Tan, H. Zhang, *Angew. Chem. Int. Ed.* **2016**, *55*, 8816; c) L. Wang, X. Zheng, L. Chen, Y. Xiong, H. Xu, *Angew. Chem. Int. Ed.* **2018**, *57*, 3454.

[10] a) P. Solís-Fernández, M. Bissett, H. Ago, *Chem. Soc. Rev.* **2017**, *46*, 4572; b) D. Jariwala, T. J. Marks, M. C. Hersam, *Nat. Mater.* **2017**, *16*, 170.

[11] a) Y. Gong, J. Lin, X. Wang, G. Shi, S. Lei, Z. Lin, X. Zou, G. Ye, R. Vajtai, B. I. Yakobson, *Nat. Mater.* **2014**, *13*, 1135; b) C. Tan, H. Zhang, *J. Am. Chem. Soc.* **2015**, *137*, 12162; c) Z. Zhang, P. Chen, X. Duan, K. Zang, J. Luo, X. Duan, *Science* **2017**, *357*, 788; d) Q. Zhang, X. Xiao, R. Zhao, D. Lv, G. Xu, Z. Lu, L. Sun, S. Lin, X. Gao, J. Zhou, *Angew. Chem. Int. Ed.* **2015**, *54*, 8957.

[12] B. Zhao, Z. Wan, Y. Liu, J. Xu, X. Yang, D. Shen, Z. Zhang, C. Guo, Q. Qian, J. Li, *Nature* **2021**, *591*, 385.

[13] S. Yang, S. Brüller, Z.-S. Wu, Z. Liu, K. Parvez, R. Dong, F. Richard, P. Samorì, X. Feng, K. Müllen, *J. Am. Chem. Soc.* **2015**, *137*, 13927.

[14] a) M.-X. Wang, C. Liu, J.-P. Xu, F. Yang, L. Miao, M.-Y. Yao, C. Gao, C. Shen, X. Ma, X. Chen, *Science* **2012**, *336*, 52; b) C. Cui, W.-J. Hu, X. Yan, C. Addiego, W. Gao, Y. Wang, Z. Wang, L. Li, Y. Cheng, P. Li, *Nano Lett.* **2018**, *18*, 1253; c) A. Ciesielski, S. Haar, M. El Gemayel, H. Yang, J. Clough, G. Melinte, M. Gobbi, E. Orgiu, M. V. Nardi, G. Ligorio, *Angew. Chem. Int. Ed.* **2014**, *53*, 10355.

[15] a) H. Shi, M. Li, A. Shaygan Nia, M. Wang, S. Park, Z. Zhang, M. R. Lohe, S. Yang, X. Feng, *Adv. Mater.* **2020**, *32*, 1907244; b) P. Marvan, V. Mazánek, Z. Sofer, *Nanoscale* **2019**, *11*, 4310.

[16] T. L. Cocker, D. Baillie, M. Buruma, L. V. Titova, R. D. Sydora, F. Marsiglio, F. A. Hegmann, *Phys. Rev. B* **2017**, *96*, 205439.

[17] Z. Liu, H. Zhang, M. Eredia, H. Qiu, W. Baaziz, O. Ersen, A. Ciesielski, M. Bonn, H. I. Wang, P. Samorì, *ACS Nano* **2019**, *13*, 9431.

[18] a) D. Pierucci, H. Henck, J. Avila, A. Balan, C. H. Naylor, G. Patriarche, Y. J. Dappe, M. G. Silly, F. Sirotti, A. C. Johnson, *Nano Lett.* **2016**, *16*, 4054; b) Q. Liu, B. Cook, M. Gong, Y. Gong, D. Ewing, M. Casper, A. Stramel, J. Wu, *ACS Appl. Mater. Interfaces* **2017**, *9*, 12728.

[19] a) W. Wang, J. Yuan, G. Shi, X. Zhu, S. Shi, Z. Liu, L. Han, H.-Q. Wang, W. Ma, *ACS Appl. Mater. Interfaces* **2015**, *7*, 3994; b) C. Lan, C. Li, S. Wang, T. He, Z. Zhou, D. Wei, H. Guo, H. Yang, Y. Liu, *J. Mater. Chem. C* **2017**, *5*, 1494.

[20] a) J. Zou, Y. Ke, X. Zhou, Y. Huang, W. Du, L. Lin, S. Wei, L. Luo, H. Liu, C. Li, K. Shen, A. Ren, J. Wu, *Adv. Opt. Mater.* **2022**, *10*, 2200143; b) S. M. Song, J. K. Park, O. J. Sul, B. J. Cho, *Nano Lett.* **2012**, *12*, 3887.

Manuscript received: March 18, 2023
Accepted manuscript online: May 10, 2023
Version of record online: ■■, ■■

Research Articles

2D Materials

H. Shi, M. Li, S. Fu, C. Neumann, X. Li, W. Niu, Y. Lee, M. Bonn, H. I. Wang, A. Turchanin, A. Shaygan Nia,* S. Yang,* X. Feng*

High-throughput Synthesis of Solution-Processable van der Waals Heterostructures through Electrochemistry

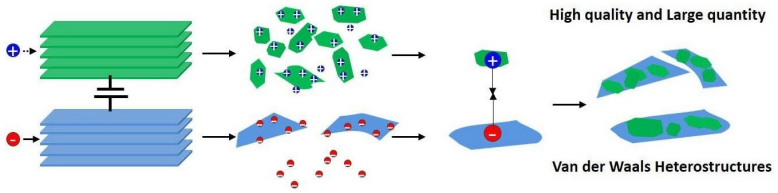

A general method is demonstrated for the preparation of high-quality van der Waals heterostructures in solution through an electrochemical strategy. The produced van der Waals heterostructures exhibit strong interlayer coupling, extraordinary structural integrity, large lateral dimension and good optoelectronic properties.